# Fast 3-D converted-wave depth-variant common conversion point stacking

Shaowu Wang, Mark C. Lane, and Don C. Lawton

## ABSTRACT

In converted-wave data processing, one of the key steps is common conversion point (CCP) stacking or binning. There are two methods of implementing CCP binning. One uses asymptotic CCP binning and the other uses depth-variant CCP binning. Although asymptotic CCP binning is simple and fast, it is only a first-order approximation of the true conversion point. Conventional depth-variant CCP binning methods are accurate for horizontally layered media. However, because a complicated expression is required and calculations must be performed at each binned time sample, the method is time-consuming.

In this paper, we develop a fast 3-D converted-wave depth-variant common conversion point (CCP) stacking method. In its implementation, source-receiver azimuth is taken into account and samples are mapped into their new CCP binning locations block-by-block, instead of sample-by-sample. We also demonstrate a modification of the algorithm, extending it to depth-variant velocity models with a constant or slowly varying ratio of *P*-wave to *S*-wave velocities. Finally, a physical modelling example demonstrates the feasibility of the new method.

## INTRODUCTION

Stacking techniques for common reflection point data are commonly used in reflection seismology to attenuate multiples and random noise and to estimate the subsurface velocity distribution. The application of this technique to converted-waves is not as simple as for conventional *P-P* or *S-S* wave reflections, which have symmetrical ray paths.

Even for simple, horizontally layered media, ray paths of *P-S* converted-waves are asymmetric, as shown in Figure 1. Multiple coverage is not achieved by a common midpoint (CMP) gather, but requires use of the true wave conversion point, yielding a common conversion point (CCP) gather (Tessmer et al, 1988).

For a single, horizontal, homogeneous layer, if the source-receiver offset is small relative to the depth of the conversion point, a first-order approximation for horizontal distance *Xp* of the conversion point from the source point can be given by

$$X_p = \frac{2h}{1+V_s/V_p}, \tag{1}$$

where $V_p$ and $V_S$ are the *P*-wave and *S*-wave velocities respectively (Slotboom et al, 1989; Tessmer et al, 1988; etc.). Binning based on equation (1) is called asymptotic CCP binning. This is a considerable improvement over CMP binning, and is computationally faster than depth-variant binning (Schafer, 1992).

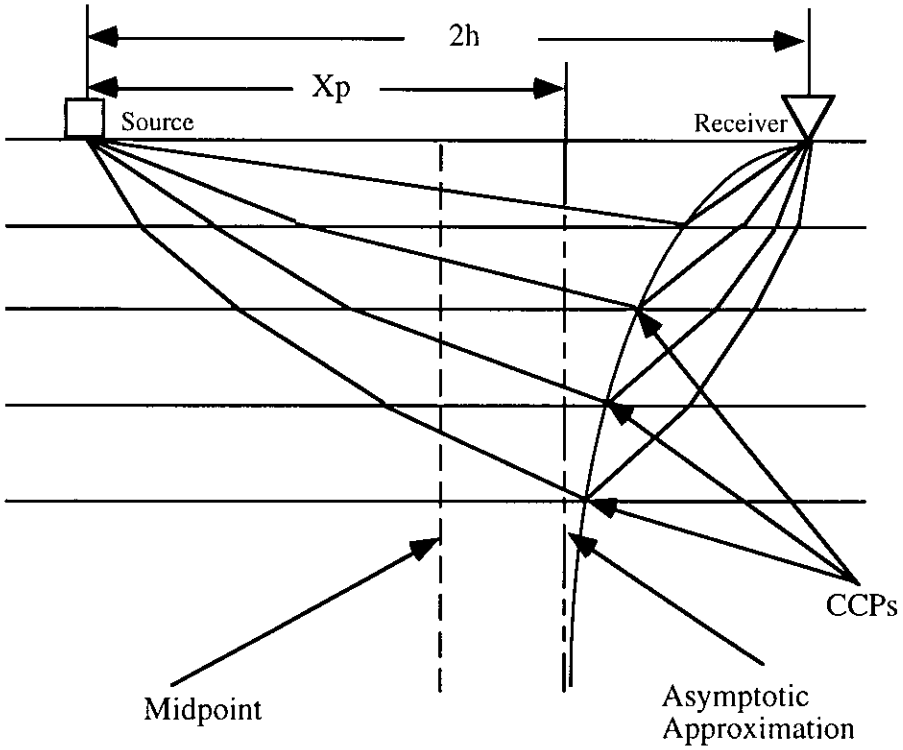


FIG. 1. Schematic diagram for 2-D common conversion point (CCP) binning.

In order to improve the asymptotic method, it is necessary to account for the depth-variance of the conversion point trajectory. Tessmer and Behle (1988) have shown that the horizontal distance D of the conversion point from the source-receiver midpoint satisfies the forth-degree polynomial equation

$$D^4+\left(z_c^2-2h^2\right)D^2-2hkz_c^2D+h^2\left(h^2+z_c^2\right)=0, \tag{2}$$

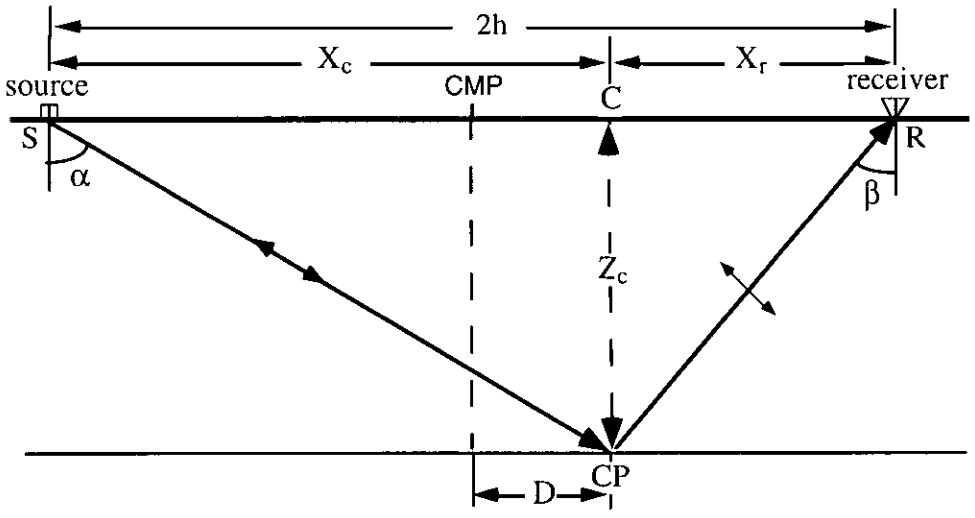


FIG. 2. The raypath of a converted-wave (*P-SV*).

where $z_c$ is the layer thickness, 2h is the source-receiver offset, as shown in Figure 2, and $k=(1+V_s/V_p)/(1-V_s/V_p)$. A unique solution of $D$, which is real and satisfies the relation $D \leq h$, can be obtained explicitly.

Recently, with the increasing interest in petrophysics and 3-D subsurface structure determination by seismic exploration, people have been giving more attention to 3-D converted-wave seismic exploration (Tatham et al, 1993). To facilitate this, several new processing algorithms must be developed. Among them is 3-D converted-wave CCP binning. Generally, the source-receiver azimuth must be taken into account. Moreover, because 3-D data sets are often very large, computing resources become an important factor in the implementation of new algorithms.

Lane and Lawton (1993) have developed a 3-D asymptotic CCP algorithm. For both 2-D and 3-D converted-wave CCP binning methods, although asymptotic CCP binning is simple and fast, it is only a first-order approximation of the true conversion point. Conventional binning parameters for asymptotic CCP binning lead to periodicities in both offset and fold (Eaton et al, 1990). Furthermore, when the source interval is an integer multiple of the group interval multiplied by the average $V_p/V_S$ ratio, empty bins occur. Although the choice of an optimum bin size can solve this problem, these bins are always larger than conventional bins with a size of half the group interval (Lawton, 1993). Tessmer and Behle's (1988) depth-variant CCP binning method is accurate for a simple horizontally layered medium. However, because the expression for D is complicated and D must be calculated for each binned time sample, the method is very time-consuming.

In this paper, we develop a fast 3-D converted-wave depth-variant common conversion point (CCP) stacking method. In its implementation, source-receiver azimuth is taken into account and samples are mapped into their new CCP binning locations block-by-block, instead of sample-by-sample. We also extend the algorithm to include a depth-variant velocity model with constant or slowly varying ratio of *P*-wave to *S*-wave velocities.

## FAST 3-D DEPTH-VARIANT CCP BINNING

Figure 3 is a schematic diagram showing how 3-D depth-variant common conversion point (CCP) stacking works, where $\phi$ is the source-receiver azimuth, ACCP is the position of asymptotic CCP locations on the surface. In this diagram, we assumed that the data have been sorted into asymptotic common conversion points using equation (1), as discussed by Lane and Lawton (1993), and NMO correction has already been applied to the data using the time-shifted hyperbolic equation given by Slotboom and Lawton (1989)

$$t = \frac{t_0}{2} + \sqrt{\frac{t_0^2}{4} + \frac{(2h)^2}{2v^2}}, \tag{3}$$

where t is the two-way travel time, $t_0$ is the zero-offset two-way travel time, 2h is the offset and v is the effective *P-SV* stacking velocity. We then re-sort the data into their true conversion point locations by 3-D converted-wave depth-variant CCP binning.

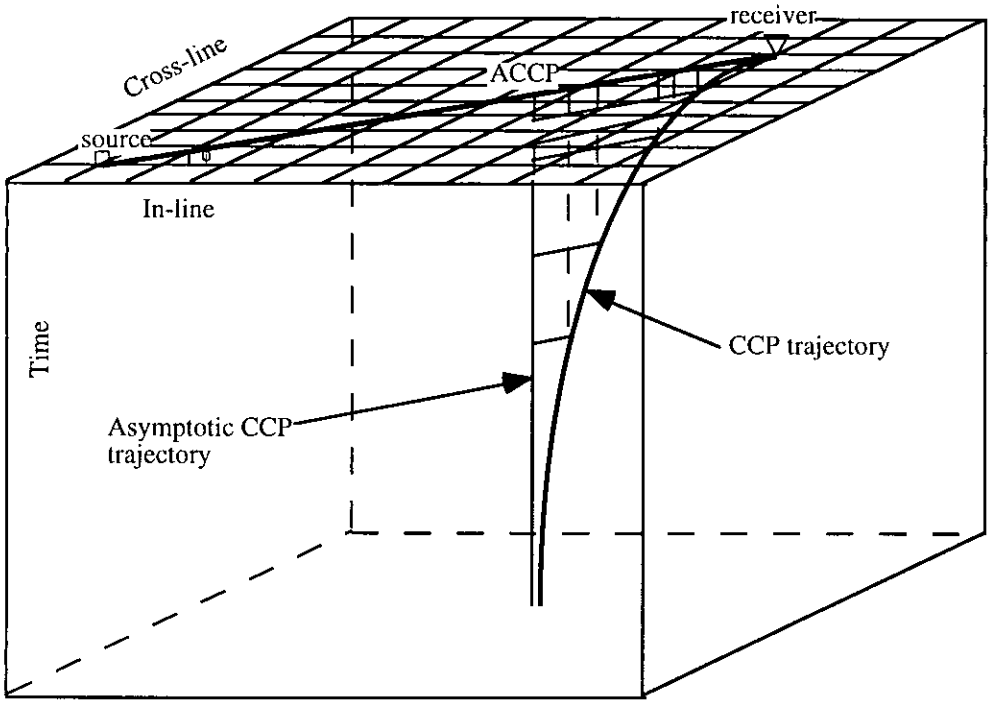


FIG. 3. Schematic diagram for 3-D depth-variant common conversion point (CCP) Binning

For a single, horizontal, homogeneous layer, as shown in Figure 2, according to Snell's law, we can derive the following relation

$$\gamma^2\left(\frac{Z_c^2}{X_c^2}+1\right)=\frac{Z_c^2}{(2h-X_c)^2}+1, \tag{4}$$

where $Z_c$ is the depth of the conversion point, $X_c$ is the horizontal distance between the conversion and source points, 2h is the source-receiver offset, and $\gamma$ is the ratio of *P*-wave to *S*-wave velocity ($V_P/V_S$). If $Z_c$ is known, then by rationalizing equation (4), we get equation (2) (Tessmer and Behle, 1988). However, if the horizontal distance of the conversion point from the source point $X_c$ is known, then the corresponding depth $Z_c$ of the conversion point can be expressed as

$$Z_c = X_c(2h-X_c)\sqrt{\frac{1-\gamma^2}{\gamma^2(2h-X_c)^2-X_c^2}}, \tag{5}$$

For a constant velocity model, the corresponding two-way travel time $t_c$ and zero-offset two-way travel time $t_{0c}$ are given by

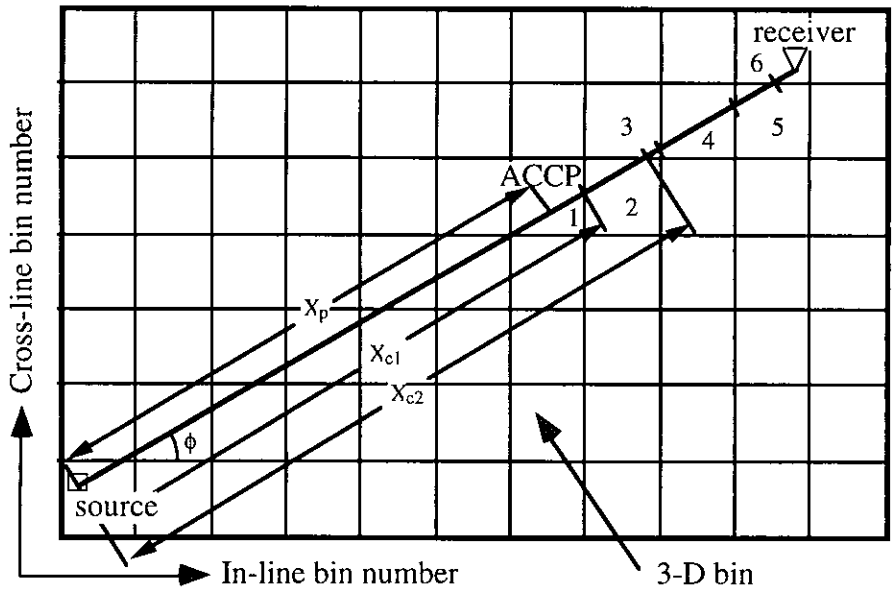


FIG. 4a. Plan view of 3-D depth-variant CCP binning scheme.

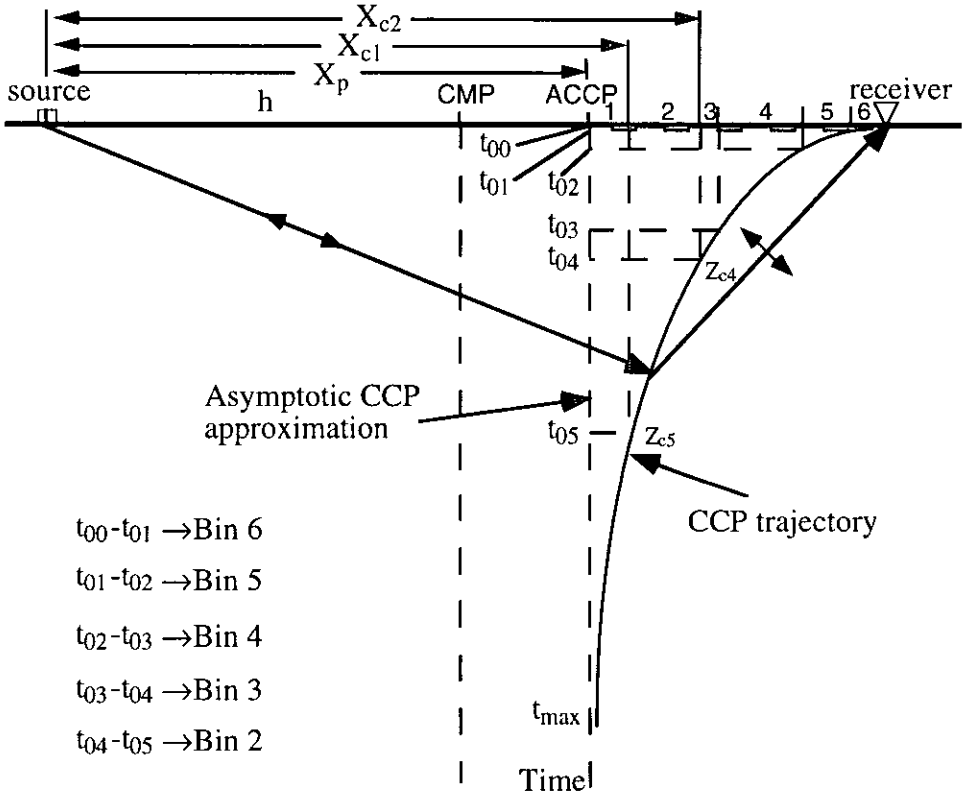


FIG. 4b. Cross-section in source-receiver azimuth direction showing how to implement 3-D depth-variant CCP binning method.

$$t_c = \frac{\sqrt{X_c^2+Z_c^2}}{V_p} + \frac{\sqrt{(2h-X_c)^2+Z_c^2}}{V_s}, \tag{6a}$$

$$t_{0c} = \frac{Z_c}{V_p} + \frac{Z_c}{V_s}, \tag{6b}$$

The algorithm has three steps. First, we find the horizontal distance $X_c$ from the conversion point to the source point; then we calculate the corresponding depth $Z_c$; finally, we map the samples to their new bins. Figure 4a and Figure 4b illustrate this procedure, showing a plan view, and a cross section from source to receiver, respectively.

Figure 4a and Figure 4b show that the true conversion point is always located horizontally between the asymptotic conversion point and receiver. The shallower the conversion point, the further the true conversion point is from the asymptotic conversion point. For each trace in a given coordinate system, the source and receiver positions are known. Once the in-line and cross-line bin sizes are chosen, all of the bin positions are fixed in this coordinate system. Given these parameters, we can locate the intersections between source-receiver line and the bin boundaries. As mentioned earlier, only these intersections between the asymptotic conversion point (ACCP) and the receiver need be considered. For example, in Figure 4a, once the two intersections between the source-receiver line and the boundary of bin 2 are found, the corresponding distances $X_{c1}$ and $X_{c2}$ can be calculated. Substituting the horizontal distance $X_c$, offset 2h and velocity ratio $\gamma$ into equation (5), the corresponding depths $Z_{c5}$ and $Z_{c4}$ for $X_{c1}$ and $X_{c2}$ can be derived respectively, as shown in Figure 4b. Zero-offset two-way travel times $t_{05}$ and $t_{04}$, corresponding to depths $Z_{c5}$ and $Z_{c4}$, are calculated using equation (6b). Finally, the samples between time interval $t_{05}$ and $t_{04}$ are relocated to their new bin number, bin 2. For the example shown in Figures 4a and 4b, the equations (5) and (6b) are solved only five times for this trace.

Based on the above discussion, compared with the conventional depth-variant CCP binning, the new depth-variant CCP binning method has the following advantages. First, the method is not only suitable for 2-D CCP binning but also for 3-D CCP binning; secondly, the derivation is very straightforward and the calculations of depth $Z_c$ from $X_c$ are simpler than that of $X_c$ from $Z_c$, so the algorithm is much faster; finally, samples are mapped to their new CCP binning locations block-by-block, instead of sample-by-sample, so it is a rapid way to implement 3-D depth-variant CCP binning method.

## MODIFICATION FOR DEPTH-VARIANT VELOCITIES

The above procedure can be generalized to include the more realistic case of a layered earth where the *P*-wave and *S*-wave velocities vary with depth. To simplify our discussion while retaining the general application of our conclusions, we assume that, although the *P*-wave and *S*-wave velocities are depth-variable, their ratio ($V_P/V_S$) is constant or only slowly varying with depth. This is a good approximation for real data at common depths of interest. We see from equation (5) that, for a given offset and horizontal distance from the conversion point to the source, only the velocity ratio $\gamma$ affects the depth $Z_c$ of the conversion point. This means that, for a given depth, velocity ratio and offset, the conversion points maintain horizontal position regardless

of *P*- and *S*-wave velocities changes. If the velocity ratio $\gamma$ changes slowly with depth, then the average velocity ratio $\bar{\gamma}$ can be used in equation (5). However, in the conversion from the depth $Z_c$ to its corresponding zero-offset two-way travel time, equations (6) are no longer suitable.

To convert from $Z_c$ to its corresponding zero-offset two-way travel time, we assume that the *P*-wave root mean square (RMS) velocity ($V_p^{RMS}$) and effective converted-wave (*P-SV*) velocity, denoted as $V_{psv}^{e}$, are available from a velocity analysis of *P*-wave and *P-SV* data. In fact, the so-called the effective *P-SV* velocity should be effective *P-SV* RMS velocity $V_{psv}^{RMS}$, which is approximately the *P-SV* stacking velocity used in the *P-SV* NMO correction, as given by equation (3).

Based on the above assumptions and definitions, the *P*-wave interval velocity ($V_p$) and effective *P-SV* interval velocity ($V_{psv}$) for each time sample can be calculated. Then the corresponding depths, $D_p$ and $D_{psv}$, for every time sample of *P*-wave and *P-SV* data can be derived using the following equations

$$D_{i+1} = D_i + \Delta t \cdot V_{i+1} \qquad \text{i=1 to NS} \qquad (7)$$
$$\textit{with}\ D_0=0,$$

where $\Delta t$ is the sample rate, i is the time sample number, NS is the total number of samples, $V_{i+1}$ is $V_p$ or $V_{psv}$ at time sample i+1, $D_{i+1}$ and $D_i$ are $D_p$ or $D_{psv}$ at the time samples i+1 and i respectively. We compute and save these $D_p$ or $D_{psv}$ values in a table for later use. For the *P*-wave and *P-SV* data, the corresponding depths ($D_p$ and $D_{psv}$) for the same time sample are different. In order to calculate the velocity ratio $\gamma$, we need the *P* and *S*-wave velocities at the same depth. By linear interpolation, the *P*-wave interval velocity at each reference depth ($D_{psv}$) can be obtained. Because we are interested in *P-SV* data processing, the reference depth is chosen to be that corresponding to each time sample of the *P-SV* data.

Now that the *P*-wave interval velocity and effective *P-SV* interval velocity at the depth corresponding to each time sample of the *P-SV* data are obtained, the next step is to calculate the *S*-wave interval velocity.

As shown in Figure 5, the layer $\Delta Z$ between i and i+1 time samples is thin. In this thin layer, the downgoing *P*-wave velocity is $V_{p(i)}$ and the upgoing *S*-wave velocity is $V_{s(i)}$. Then the effective *P-SV* interval velocity $V_{psv(i)}$ has the following

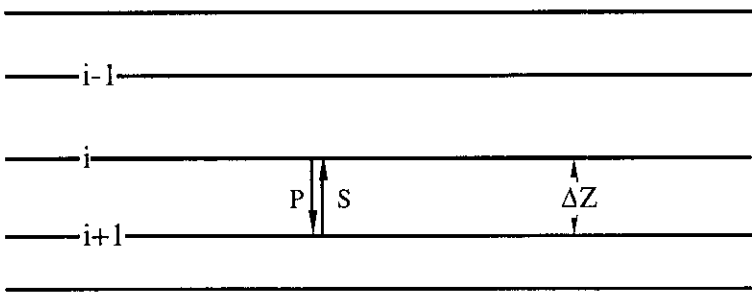


FIG. 5. The diagram showing the relationship of effective *P-SV* velocity and *P*- and *S*-wave interval velocities.

relationship with the thickness $\Delta Z$, *P*-wave velocity $V_{p(i)}$ and *S*-wave velocity $V_{s(i)}$,

$$\frac{2\Delta Z}{V_{psv(i)}} = \frac{\Delta Z}{V_{p(i)}} + \frac{\Delta Z}{V_{s(i)}}, \tag{8}$$

Simplifying the above equation, we can get $V_{s(i)}$ as

$$V_{s(i)} = \frac{V_{psv(i)} V_{p(i)}}{2V_{p(i)} - V_{psv(i)}}, \tag{9}$$

With this derived *S*-wave interval velocity, $V_P/V_S$ for each depth, corresponding to each time sample of *P-SV* data, can be derived simply by

$$\gamma_{(i)} = \frac{V_{p(i)}}{V_{s(i)}}, \tag{10}$$

In equation (4) or equation (5), in order to calculate the depth $Z_c$ for a given offset (2h) and horizontal distance from the conversion point to the source point ($X_c$), we need the average velocity ratio ($\bar{\gamma}$) from the surface to this depth, if $\gamma$ changes with depth. This gives rise to the question of how we can get $\bar{\gamma}$ without already knowing $Z_c$. To deal with this problem, we use the following approximation technique. As shown in Figure (4b) and discussed above, before the calculation of $Z_{c4}$ , the depth $Z_{c5}$ has already been calculated. The average velocity ratio $\bar{\gamma}$ at depth $Z_{c5}$ is used in equation (5) to calculate the depth $Z'_{c4}$, which is the first-order approximation for the true depth $Z_{c4}$. Given the calculated depth $Z'_{c4}$, an updated average velocity ratio $\bar{\gamma}$ at $Z'_{c4}$ can be calculated. Substituting this new average velocity ratio $\bar{\gamma}$ into equation (5), the second-order approximation for the true $Z_{c4}$ can be obtained. Generally speaking, as indicated in our assumptions, the velocity ratio ($\gamma$) changes slowly with depth, so the second-order approximation can match the true depth $Z_{c4}$ adequately.

The conversion of depth $Z_c$ into its corresponding zero-offset two-way travel time is very simple. As mentioned early, for each time sample of *P-SV* data, the depth $D_{psv}$ is already calculated and saved in a table. By looking in this table, the zero-offset two-way travel time $t_0$, corresponding the calculated depth $Z_c$, can be found.

## EXAMPLE OF 3-D CONVERTED-WAVE PHYSICAL MODEL

These algorithms were applied to data generated over a scaled physical model. The model consists of a rectangular-shaped cavity milled into the base of a layer of plexiglas of 9.8 cm thick, with *P*-wave velocity of 2750 m/s and *S*-wave velocity of 1375 m/s. The cavity is about 1.4 cm deep, 8.0 cm long, 5.0 cm wide and is air-filled. World units are shown using a distance scaling factor of 10,000:1. The cross-sections of the model are shown in Figure 6.

A three-dimensional, three-component data set was acquired over the model using the elastic physical modeling system at The University of Calgary, using a *P*-wave transducer as the source. A plan view of the survey is shown in Figure 7, with all

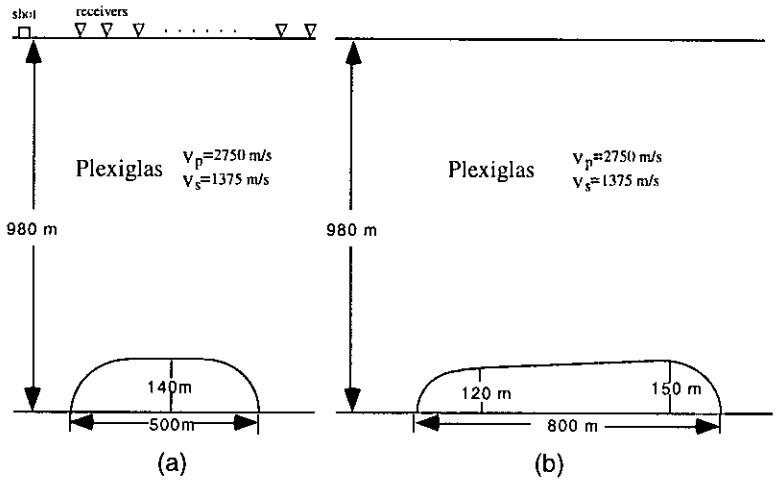


FIG. 6. The cross-sections of the model in receiver-line (a) and shot-line (b) directions across the middle of the model.

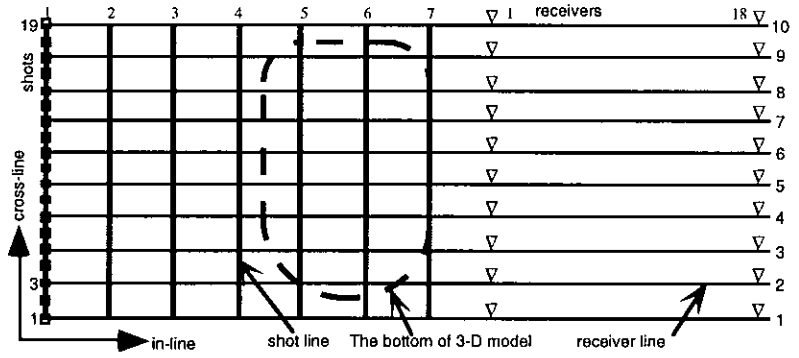


FIG. 7. The plan view of model showing acquisition geometry.

dimensions shown after a distance scaling factor of 10,000:1 has been applied. There were 7 shot lines with line spacing of 200 m, 19 shots per shot-line and shot spacing of 50 m. For each shot, data were acquired along 10 receiver lines with a spacing of 100 m, a near offset of 200 m, 18 receiver stations per receiver line and a receiver spacing of 50 m. The sample rate was 1 ms and the recorded length was 1.5 s. The survey was repeated three times to enable vertical, in-line and cross-line receiver components to be collected. Here, in-line refers to receiver line direction and cross-line refers to shot-line direction.

The fold map of asymptotic CCP binning of the *P-SV* data for the above geometry is shown in Figure 8. In this figure, the bin sizes in the in-line and cross-line directions are half of the receiver interval. From this fold map, it is seen that for every four rows in receiver-line direction there is an empty row of bins. This is because when a conventional common midpoint bin size of half the receiver interval ($\Delta r/2$) is used, the fold distribution is highly variable and empty rows of bins parallel to the shot lines may result for the case when $V_p/V_s=2$ and the shot line spacing is an even integer multiple of $\Delta r$ (Lawton, 1993). Figures 9a-9e are the fold maps of depth-variant common conversion point binning at different zero-offset two-way travel time. The fold maps in these figures are more evenly distributed than those of asymptotic CCP binning, especially for later times. Although the bin size is still half of the receiver

interval, there are no empty rows of bins. From early time (0.2 s) to late time (1.0 s), as the time and depth increases, the fold map becomes more evenly distributed. Due to hardware constraints in data acquisition, the sources were always on the left side of the receivers. This pushed higher folds in the direction of the source, as time and depth increase.

A sample section of *P-SV* stacked data in the receiver-line direction with a bin size of 25 m using asymptotic common conversion binning method is shown in Figure 10. Again, we can see that every fourth traces is empty. It's counterpart using depth-variant common conversion point binning is shown in Figure 11. In this case, the reflection events are more continuous. This stacked section is improved and the lateral resolution is increased.

## CONCLUSIONS

Based on the above discussions, the following conclusions can be reached,

(1) In order to improve the stacked section of the converted-wave data, whether for 2-D or 3-D, depth-variant common conversion point stacking is necessary. The fast 3-D converted-wave depth-variant CCP stacking method described in this paper provides an efficient and easy way to achieve this goal.

(2) The implementation gains considerable speed through the mapping of samples in blocks instead of individually.

(3) With reasonable constraints on velocities and their ratio, the algorithm was modified to deal with depth-variant velocity model.

(4) A 3-D converted-wave physical model has demonstrated the feasibility of the new method.

## ACKNOWLEDGMENTS

The authors would like to thank Mr. G. A. Larson for his helpful discussions. We would also like to thank the sponsors of The CREWES Project.

## REFERENCES

Eaton, D.W.S., and Lawton, D.C., 1990, *P-SV* stacking charts and binning periodicity: CREWES Research Project, 2, 36-44.

Lane, M, and Lawton, D.C., 1993, 3-D converted wave asymptotic binning: CREWES Research Project, 5, 29, 1-25.

Lawton, D.C., 1993, Optimum bin size for converted-wave 3-D asymptotic mapping: CREWES Research Project, 5, 28, 1-12.

Schafer, A.W., 1992, A comparison of converted-wave binning methods using a synthetic model of the Highwood structure, Alberta: CREWES Research Project, 4, 9, 1-9.

Slotboom, R.T., and Lawton, D.C., 1989, Depth-variant mapping and moveout correction of converted-wave data: CREWES Research Project, 1, 55-65.

Tatham, R.H., and Stewart, R.R., 1993, Present status and future directions in application of shear-wave seismology in exploration: CREWES Research Project, 5, 1, 1-19.

Tessmer, G., and Behle A., 1988, Common reflection point data stacking technique for converted waves: Geophysical Prospecting, 36, 671-688.

Tessmer, G., Krajewski, P., Fertig, J., and Behle, A., 1990, Processing of P*S*-reflection data applying a common conversion-point technique: Geophysical Prospecting, 38, 267-286.

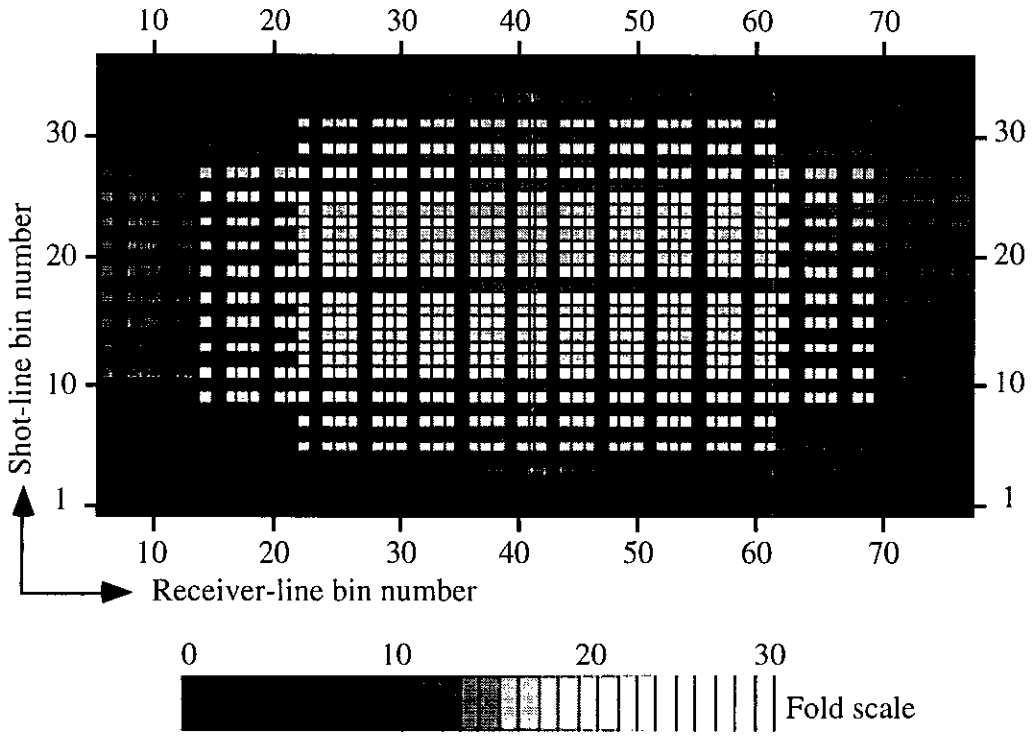


FIG. 8. Fold map of asymptotic common conversion point binning with bin size 25 m.

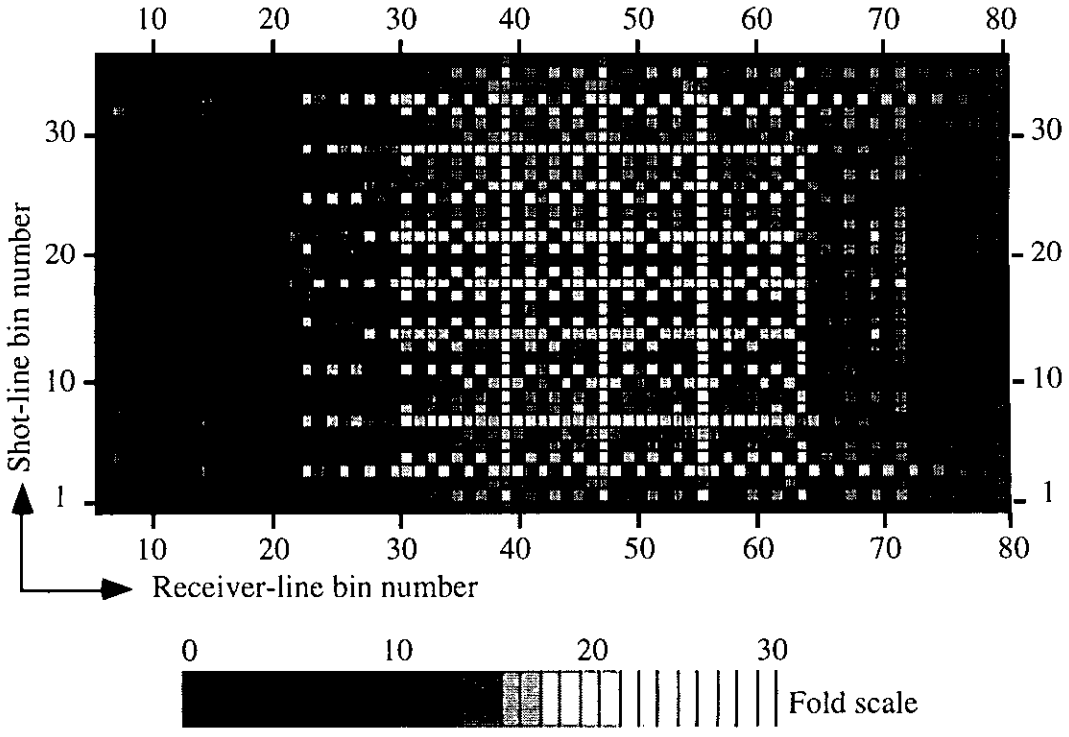


FIG. 9a. Fold map of depth-variant common conversion point binning with bin size 25 m, time=200 ms.

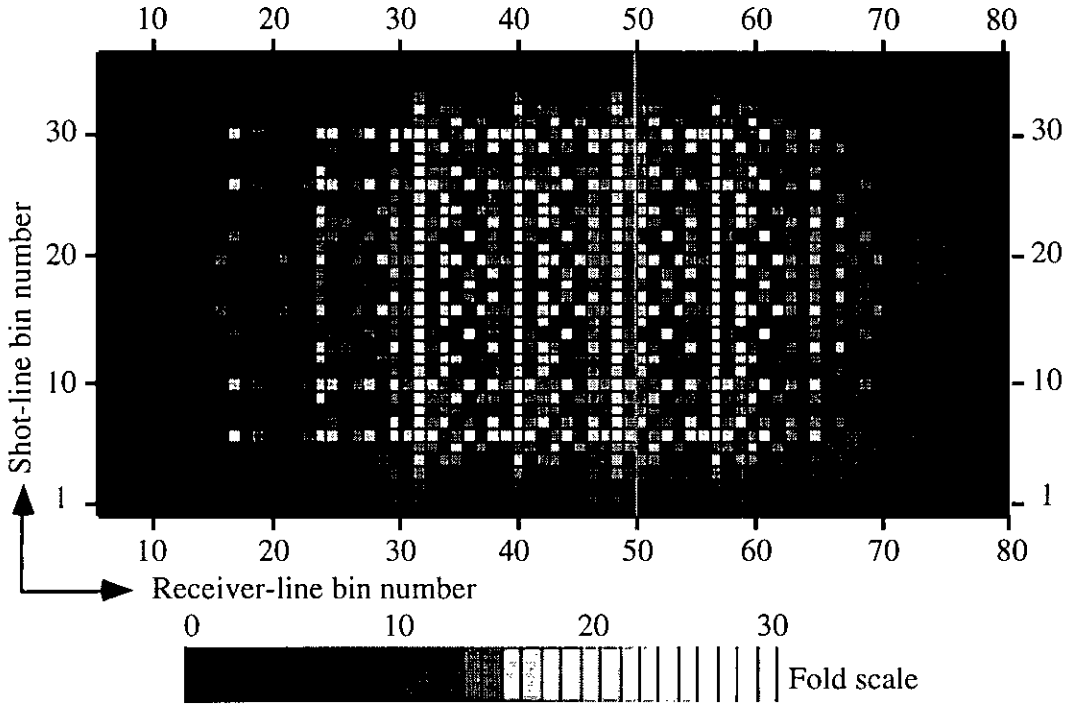


FIG. 9b. Fold map of depth-variant common conversion point binning with bin size 25 m, time=400 ms.

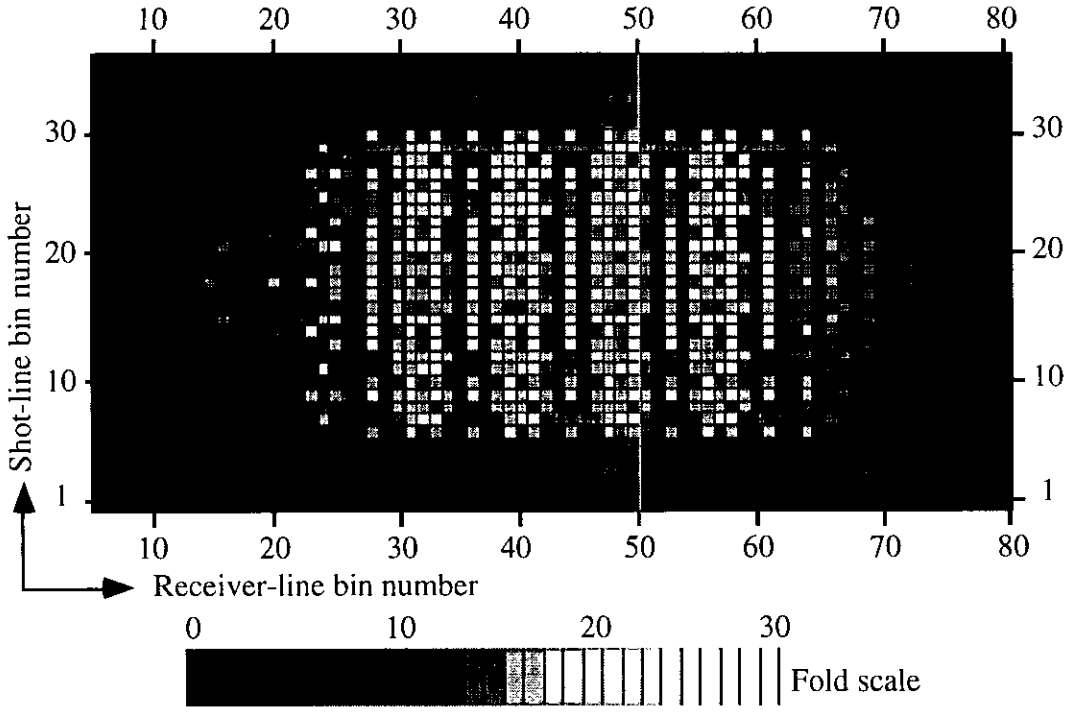


FIG. 9c. Fold map of depth-variant common conversion point binning with bin size 25 m, time=600 ms.

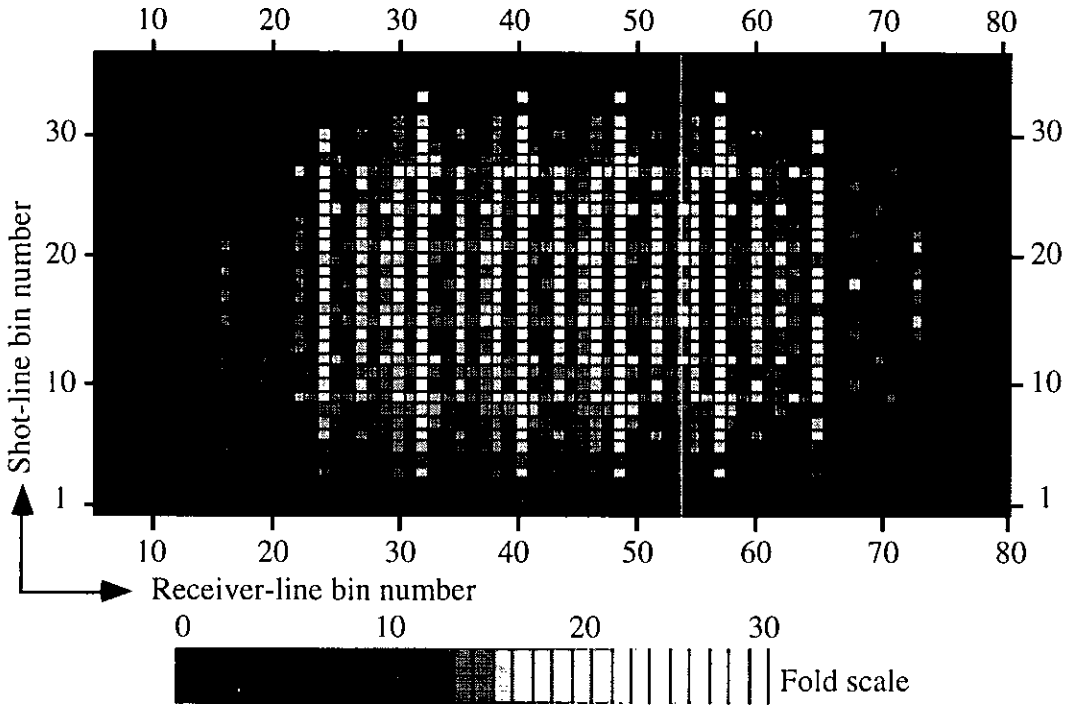


FIG. 9d. Fold map of depth-variant common conversion point binning with bin size 25 m, time=800 ms.

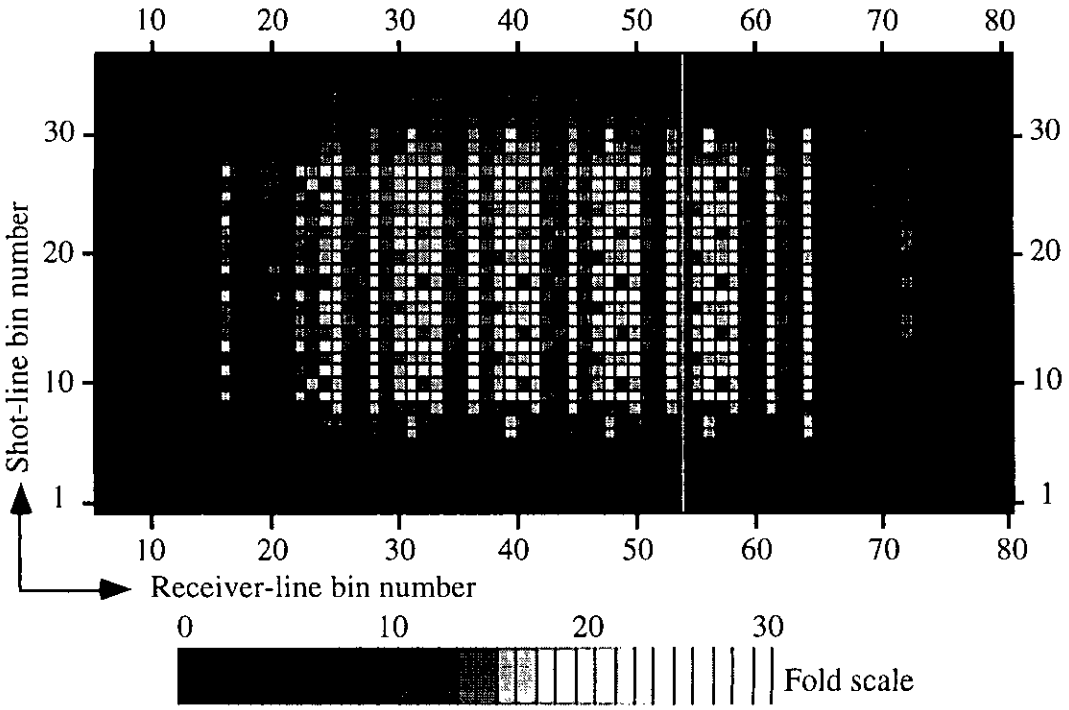


FIG. 9e. Fold map of depth-variant common conversion point binning with bin size 25 m, time=1000 ms.